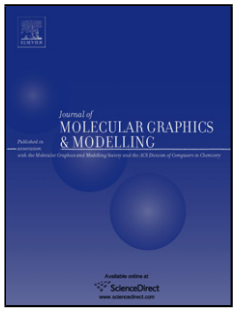

Title: Hydrogen generation from methylamine using silicon carbide nanotubes as a dehydrogenation catalyst: A density functional theory study

Author: Mehdi D. Esrafili Roghaye Nurazar

PII: S1093-3263(14)00182-X
DOI: http://dx.doi.org/doi:10.1016/j.jmgm.2014.11.005
Reference: JMG 6484

To appear in: *Journal of Molecular Graphics and Modelling*

Received date: 24-6-2014
Revised date: 13-10-2014
Accepted date: 7-11-2014

Please cite this article as: M.D. Esrafili, R. Nurazar, Hydrogen generation from methylamine using silicon carbide nanotubes as a dehydrogenation catalyst: A density functional theory study, *Journal of Molecular Graphics and Modelling* (2014), http://dx.doi.org/10.1016/j.jmgm.2014.11.005

Highlights

1- The adsorption and decomposition of CH_3NH_2 on the SiCNT is studied.

2- SiCNTs can be used as a metal-free catalyst for CH_3NH_2 dehydrogenation.

3- For the dehydrogenation of CH_3NH_2 on the SiCNT surface, the rate-determining step is $HCNH \rightarrow HCN + H$.

Graphical abstract

. Hydrogen generation from methylamine using SiCNTs as a dehydrogenation catalyst

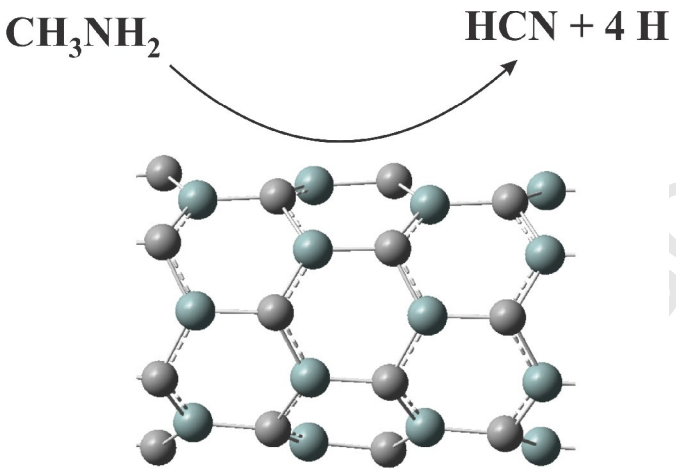

Hydrogen generation from methylamine using silicon carbide nanotubes as a dehydrogenation catalyst: A density functional theory study

Mehdi D. Esrafili* and Roghaye Nurazar

Laboratory of Theoretical Chemistry, Department of Chemistry, University of Maragheh, Maragheh, Iran

* Corresponding author. **Phone:** (+98) 4212237955. **Fax:** (+98) 4212276060. **P.O. Box:** 5513864596**. E-mail**: esrafili@maragheh.ac.ir (Mehdi D. Esrafili).

Abstract

The adsorption and decomposition of methylamine on the surface of a pristine silicon-carbide nanotube (SiCNT) are investigated by density functional theory calculations. The adsorption energies of possible stable configurations and the activation energies for possible elementary reactions involved are obtained in the present study. The most favorable reaction channel that generates a hydrogen cyanide molecule and four hydrogen atoms is slightly endothermic; the energy barrier for the decomposition of the CH_3NH_2 molecule is about 45 kcal/mol. Since the activation energy for the side reaction that generates CH_3 and NH_2 fragments is relatively high, the generation of side products may be depressed by decreasing the temperature.

Key words: SiCNT; methylamine; DFT; decomposition; catalysis.

1. Introduction

For its environmental and economic reasons, hydrogen fuel has been considered to be an efficient and alternative secondary energy resource particularly when is combined with fuel-cell technology [1,2]. However, the future application of hydrogen-based energy is limited by the lack of a convenient, cheap and safe storage system. An efficient hydrogen storage material should possess fast sorption kinetics, high volumetric/gravimetric density, relatively low dehydrogenation temperatures for chemical hydrides [3,4], and the hydrogen adsorption energy must be in the range of -0.2 to -0.7 eV at room temperature [5]. The first requirement limits the choice of storage materials to be composed of lighter elements, while the latter requires hydrogen binding energies to be between physisorption and chemisorption energies. To achieve these challenging goals, several different techniques have been proposed for hydrogen storage including liquid H_2 at cryogenic temperature, into metal hydrides [6,7], and adsorbed in organic polymers [8,9]. At present, all these storage methods are used or under study; however, most of them have disadvantages in terms of toxicity, price, and safety. Hence, there is currently extensive interest in developing new and efficient hydrogen storage materials for on-board applications [10].

Among the potential hydrogen storage materials, methylamine (CH_3NH_2) and other organometalic compounds have attracted considerable attention owing to their relatively high hydrogen density and possibility to liberate H_2 in room conditions in the presence of a metal catalyst [11-13]. The total weight percentage of hydrogen contained in methylamine is about 16%, higher than that of methanol (12.5%). Furthermore, CH_3NH_2 liquefies at normal conditions, thus it can be handled and stored more easily than hydrogen. Up to now, it is well-known that methylamine can be adsorbed through the nitrogen lone pair electrons on metal surfaces [14-21], and the C–H, N–H or C–N bond can be activated at an enough high temperature. Several fundamental studies indicated that CH_3NH_2 is able to release hydrogen via a room temperature dehydrogenation reaction in the presence of a suitable catalyst [22,23]. Complete decomposition of CH_3NH_2, leading to the evolution of gaseous phase H_2, N_2 and NH_3, has been studied on W(100) surface [24]. It was indicated that the decomposition of CH_3NH_2 to produce H_2 and HCN is favored on (1×1)Pt(100), while reversible adsorption of CH_3NH_2 is the dominant reaction on (5×20)- Pt(100) [25]. Chen and Winograd [26] indicated that the C–H

bonds are more stable than the N–H bonds on Pd and Pt, whereas the Ni preferentially breaks the C–H bonds at the initial stages of the decomposition of CH_3NH_2. For the adsorption and dehydrogenation of CH_3NH_2 over Mo catalyst [27], experimental results demonstrated that CH_3NH_2 adsorbs through the interaction of the lone pair of electrons on the nitrogen atom with Mo centers present at the surface and can be catalytically decomposed into H_2 and NH_3. Yet, the high costs and toxicity of the transition metal-based catalysts might greatly limit their applications for CH_3NH_2 decomposition. In recent years, there has been an increasing amount of literature on designing new catalysts or additives to solve these problems.

Recently, we reported a density functional theory (DFT) study of using a fullerene-like $B_{12}N_{12}$ nanocage as a metal-free catalyst in decomposition of CH_3NH_2 [28]. According to our work, the $B_{12}N_{12}$ nanocage can be used as an effective catalyst to take the first N–H hydrogen atom off methylamine molecule to form CH_3NH fragment. However, the performance of the $B_{12}N_{12}$ nanocage as a catalyst used for dehydrogenation of adsorbed CH_3NH decomposition is poor and must proceed in relatively high temperature. In the present study, a new approach to catalyze the dehydrogenation of the CH_3NH_2 molecule using silicon-carbide nanotubes (SiCNTs) is introduced. These nanotubes have been found to be semiconducting materials of great technological interest for devices designed to operate at high temperatures, at high power, and in harsh environments [29,30]. More interestingly, SiCNTs have higher surface reactivity than carbon nanotubes (CNTs) or boron-nitride nanotubes (BNNTs) due to their great polarity of Si–C bonds [31,32]. In terms of these outstanding properties, an inspiration then rises: can SiCNTs be used as a metal-free catalyst for CH_3NH_2 dehydrogenation? If can, what is the reaction pathways and possible intermediates for this process? In this work, by performing DFT calculations, we would address the above questions.

2. Computational details

All DFT calculations were carried out with the GAMESS suite of programs [33]. A truncated (6,0) SiCNT with 36 Si and 36 C atoms was chosen as the basic model for the calculations. In order to avoid the boundary effects, atoms at the open ends of the tube are saturated by hydrogen atoms. It is important to note that the size of model considered for studying the properties of electronic structures of the SiCNT was validated by results from previous NMR calculations [34]. The geometries of the monomers and complexes were fully

optimized at the CAM-B3LYP/6-31G* level of theory. CAM-B3LYP is a long-range corrected version of B3LYP which includes exact Hartree-Fock exchange at long distances [35]. There are many reports that indicate CAM-B3LYP gives improved charge transfer excitation energies, reaction barriers and, in general, minimize self-interaction error over the most popular methods, e.g. B3LYP [36,37]. All structures have been fully optimized with 10^{-8} hartree as SCF convergence criterion and 10^{-6} hartree/bohr and hartree/degree, respectively, as convergence criterion for the gradient optimization of the structure. Corresponding vibratinal frequencies were computed in the harmonic approximation to identify equilibrium and transition structures. All the transition state structures were characterized by exhibiting the existence of a single frequency mode associated with a pure imaginary frequency. Intrinsic reaction coordinate (IRC) calculations were performed in the forward and reverse directions to determine minimum-energy pathways. Assessment of the transition states and energy barriers are performed at the CAM-B3LYP/6-31G* level of theory. IRC calculations were carried out starting from each transition state in order to link reactants and products. The calculations were allowed to follow the energy profile in both forward and reverse directions from the maxima and the number/size of steps was optimized for each calculation to ensure that the correct transition state has been located.

The adsorption energy (E_{ads}) of the CH_3NH_2 on the SiCNT surface is defined as follows:

$$E_{ads} = E_{CH3NH2\text{-}SiCNT} - E_{CH3NH2} - E_{SiCNT} \quad (1)$$

where $E_{CH3NH2/SiCNT}$, E_{CH3NH2}, and E_{SiCNT} are the total energy of CH_3NH_2-SiCNT complex in the equilibrium state, the energy of a single CH_3NH_2, and the energy of the free SiCNT, respectively. All E_{ads} values were obtained at the CAM-B3LYP/6-31G* level. Natural population analysis (NPA) [26] was performed at the CAM-B3LYP/6-31G* level. Electron density difference maps were obtained at the B3LYP/6-31G* level of theory.

3. Results and discussion

3.1. Adsorption of CH_3NH_2 molecule on surface of the SiCNT

Figure 1 indicates the optimized structure of the pristine (6, 0) zigzag SiCNT. The lengths of the Si–C bonds are about 1.83 (axial) and 1.76 Å (zigzag), consistent with the previous reports [38]. The NPA charge density analysis reveals that the carbon atoms are negatively charged by about -1.9 e, and that the silicon atoms are positively charged with the same magnitude. Thus,

the silicon atom (electron deficient) can be viewed as a Lewis acid, whereas the carbon atom (electron rich) plays the role of a Lewis base. In the optimized free CH_3NH_2 molecule, the C–N bond length is 1.46 Å, and the N–H and C–H bond lengths are about 1.02 and 1.09 Å, respectively.

As is well-known, the initial adsorbed state of a molecule on the catalyst surface greatly affects the subsequent catalytic reactions. To better understand the catalytic reactivity of the SiCNT toward methylamine molecule, the adsorption of CH_3NH_2 on the tube surface has been considered. The most stable configurations are shown in Figure 1 and their energetic data are listed in Table 1. In the configuration **A**, which is the most stable mode, CH_3NH_2 is adsorbed on the SiCNT surface through its nitrogen lone pair electrons in a top configuration with an adsorption energy of -45.6 kcal/mol. The Si–N bond length is about 1.94 Å, which is shorter than the corresponding interaction on Ni surface [15]. The C–N bond length of CH_3NH_2 is about 1.48 Å, a little longer than that of the isolated molecule (1.46 Å), suggesting that adsorption process weakens the C–N bond. The N–H distance is elongated from 1.02 Å in free CH_3NH_2 molecule to 1.04 Å in the complex **A**. Clearly, the CH_3NH_2 molecule on the surface of the SiCNT has been activated. As evident from Table 1, the adsorption process to form complex **A** is an exothermic reaction (ΔH_{298}=-38.5 kcal/mol), with a negative ΔG_{298} value of about -26.4 kcal/mol. The NPA indicates that the charge transfer from the nitrogen lone pair of CH_3NH_2 to the empty orbital of the Si atom in the SiCNT is 0.29 e.

In the physisorption configuration **B**, the C–N bond of the CH_3NH_2 molecule is approximately parallel to the tube with the amine hydrogen close to the surface. The distances of $NH\cdots C_{surface}$ and $CH\cdots C_{surface}$ between the CH_3NH_2 and tube surface are found to be 2.67 and 3.21 Å, respectively, and the adsorption process is slightly exothermic (E_{ads}=-1.6 kcal/mol, ΔH_{298}= -2.5 kcal/mol). However, the calculated positive ΔG_{298} value indicates that the formation of this complex is an endergonic reaction and the complex being thermodynamically unstable in the gas phase at 298 K. The C–H bond lengths are slightly elongated from 1.09 Å in free CH_3NH_2 molecule to 1.11 Å in the adsorption complex. Besides, the relatively small adsorption energy of configuration **B** for CH_3NH_2 adsorption can also be supported by a negligible charge transfer q_{CT} value (0.07 e).

To investigate the changes of electronic structures in the SiCNT caused by adsorption of CH_3NH_2 molecule, total density of states (TDOS) and projected density of states (PDOS) of the

pristine SiCNT and CH_3NH_2–SiCNT complexes are calculated and shown in Figure 1. For the pristine tube, which is a semiconductor, our DFT calculation obtains a band gap of 1.94 eV, compared to 1.42 eV reported by Wang et al. [40]. When one CH_3NH_2 molecule is chemically adsorbed on the tube, the value of the local energy levels occurs near the Fermi levels is slightly enhanced and the band gap of the system increases by 0.30 eV. As also evident from Figure 1, there are many peaks in the range of -18 to -10 eV in the DOS of the complex **A**, showing the strong hybridization between the orbitals of the nanotube and methylamine. Moreover, we note that the values of PDOSs near the Fermi level of the adsorbed CH_3NH_2 in configuration **B** are slightly higher than those of configuration **A**, which indicates that the electronic properties of the tube are sensitive to the CH_3NH_2 adsorption.

We have further calculated the electron density difference $\Delta\rho$ for the CH_3NH_2–SiCNT complexes with respect to the separated SiCNT and CH_3NH_2 fragments in order to comprehend the nature of the CH_3NH_2–SiCNT bonding characteristics. This illustrates how the charge density changes during the adsorption process. $\Delta\rho$ is defined as:

$$\Delta\rho=\rho(CH_3NH_2/SiCNT) - \rho(SiCNT) - \rho(CH_3NH_2) \quad (2)$$

where $\rho(CH_3NH_2$–SiCNT), ρ(SiCNT), and $\rho(CH_3NH_2)$ indicate electron density of SiCNT adsorbed system, SiCNT, and an isolated CH_3NH_2 molecule for the adsorbed system, respectively. The isosurfaces for the charged density difference are plotted in Figure 2, where loss of electrons is indicated in red, while electron enrichment is indicated in blue. The isodensity value shown in the figure is 0.001 e/bohr^3. For the configuration **A**, the nearest Si atom of SiCNT gains electrons while N atom of the methylamine loses electrons, which subsequently lead to the lengthening of the C–N bond of CH_3NH_2. Remarkably, some charges accumulate around the bond of Si–N, which confirm the binding between CH_3NH_2 and SiCNT induced by adsorption. The pronounced charge density redistribution and the C–N bond lengthening of methylamine on the tube surface indicate a significant interaction between the CH_3NH_2 and SiCNT. The electron density difference maps also show that there is considerable charge transfer and electron density rearrangement associated mainly with C–H$\cdots S_{surface}$ and N–H$\cdots C_{surface}$ hydrogen bonds in the configuration B. These results are supported by data from the NPA charge analysis, where charge of surface Si atom accumulates from 1.9 e to and 1.88 e and that of C atom increase from -1.90 to -1.91 e.

3.2. Decomposition of CH_3NH_2 molecule on surface of the SiCNT

Next, we study the decomposition of CH_3NH_2 on the SiCNT surface. Since CH_3NH_2 has three different kinds of heteroatom bonds, namely N–H, C–H and C–N, the decomposition step involves the breaking of these three bonds. Considering the significant difference on the adsorption energy between the two adsorption modes of CH_3NH_2, almost all the CH_3NH_2 molecules adsorb via top configuration (**A**), so decomposition of CH_3NH_2 will be studied using the complexes **A** as the initial state. The energy profiles for the different reaction pathways R1 and R2 of CH_3NH_2 dissociation over the SiCNT are shown in Figure 3. IRC calculations were performed in the forward and the reverse directions to verify the transition states. The structures of the various stationary points located on the potential energy surface are depicted in Figures 4 and 5, along with the values of the most relevant geometrical parameters. The corresponding activation energies (E_{act}), imaginary frequencies (ν), reaction energies (ΔE), reaction Gibbs free energy changes (ΔG_{298}), and enthalpy changes (ΔH_{298}) are summarized in Table 2.

The reaction pathway R1 involving TS-1 breaks the N–H bond of the CH_3NH_2 in configuration **A** and the resulting stationary structures are shown in Figure 4. The calculations reveal that the decomposition of CH_3NH_2 into adsorbed CH_3NH and H on the SiCNT surface has an activation barrier of 7.0 kcal/mol. Remarkably, this energy-barrier is much lower than those obtained by catalysis using Mo (100) surface (ca. 26.4 kcal/mol) [20] and $B_{12}N_{12}$ nanocage (ca. 30.9 kcal/mol) [28]. This indicates that the SiCNT can effectively split the N–H bond of methylamine. For the reaction path taking place through TS-1, IRC calculations in the forward direction yielded the product P1 (Figure 4). The resulting transition state TS-1 has a six-member ring structure, where the hydrogen is transferred between the nitrogen atom of methylamine and SiCNT. In the TS-1, the lengths of the H···N and H···$C_{surface}$ bonds are 1.33 and 1.52 Å, respectively. The distance from the N to the surface Si atom is 1.85 Å, shorter than its initial value in **A**, 1.94 Å, which indicates that the nitrogen atom of CH_3NH_2 in the TS-1 approaches closer to the tube surface. As the N–H bond is cleaved, product P1 is obtained. In the optimized P1 structure, the length of newly formed C–H bond is 1.10 Å, a little longer than 1.09 Å in free methane. Compared with TS-1, in P1, the nitrogen atom is further closer to the surface.

It should be noted that the possibility of CH_3NH_2 dehydrogenation through C–H bond activation is also considered. All attempts to locate a transition state for the C–H bond cleavage of CH_3NH_2 were unsuccessful; leading to conclusion that C–H bond activation through the $CH_3NH_2 \rightarrow CH_2NH_2 + H$ reaction path is either unlikely, or unable to compete with the N–H

bond cleavage. Besides, these results show that the C–H bonds are more stable than the N–H bonds over the SiCNT surface. This is in agreement with the pathway identified for dehydrogenation of CH_3NH_2 over Pd and Pt surfaces [26].

The decomposition of adsorbed CH_3NH may proceed along two pathways, $CH_3NH \rightarrow CH_3N + H$ and $CH_3NH \rightarrow CH_2NH + H$. However, the calculations predict that the latter pathway is preferable. Starting from the P1, the C–H bond cleavage of CH_3NH takes place through a transition state (TS-2) to achieve the cleaved product (P2). The unique imaginary frequency of the transition state TS-2 is 645i cm^{-1}, which has been further confirmed by the IRC calculations. In the TS-2, the methyl H atom moves toward the top site of surface Si atom, accompanied by an elongation of C–H bond length to 1.42 Å. Meanwhile, the N–Si bond between the CH_3NH and surface is elongated to 1.84 Å, which is about 0.11 Å longer than that of P1. A close examination of the optimized TS-2 structure indicates that the corresponding C–N bond distance is also shortened by 0.11 Å with respect to the CH_3NH_2 gas phase structure (1.46 Å). The activation barrier of C–H bond breaking is calculated to be 13.4 kcal/mol, the reaction is exothermic and thermodynamically favored (ΔH_{298}=-3.3 and ΔG_{298}=-3.0 kcal/mol), with a reaction energy of -27.0 kcal/mol with reference to the reactants. In the final state (P2), the hydrogen atom sits on the top site of Si atom at surface, with a Si–H bond length of 1.49 Å. The CH_2NH group also resides at Si top site on the surface; with a N–Si bond distance of 1.94 Å. Product P3 is formed from P2 through a transition state TS-3. As Figure 4 indicates, the elongation of the C–H bond of the CH_2NH moiety leads to the formation of TS-3. In TS-3, the length of C···H bond is 1.56 Å, implying that the cleaved C–H bond is too close to be dissociated. An imaginary frequency of 1187i cm^{-1} in the transition state TS-3 is associated with mode of C−H bond breaking. After the transition state TS-3 is passed, rotation of the CHNH group occurs to remove unfavorable steric interactions between the C–H moiety and the nanotube surface. Unlike the $CH_3NH \rightarrow CH_2NH$ dehydrogenation reaction, the reaction is calculated to be endothermic in the gas phase, and it needs to overcome an energy-barrier height of 25.8 kcal/mol, relative to P2. The difference in the reaction energy between the CH_3NH and CH_2NH dehydrogenation paths appears to mostly originate in the stability of the latter over the nanotube surface. As the C–H bond elongates, the hydrogen atom of N–H bond shifts to the adjacent carbon on the surface and the N–Si distance becomes 1.87 Å. In the product P3, the N–Si and C–N bond lengths are shortened to 1.82 and

1.31 Å, respectively. The reaction that proceeds from P2 to P3 is calculated to be endothermic and thermodynamically unfavorable at 298 K (ΔH_{298}=20.8 kcal/mol and ΔG_{298}=20.9 kcal/mol).

Further, the configuration P3 can be dehydrogenated to produce a hydrogen cyanide (HCN) molecule and a hydrogen atom. IRC calculations were run starting from transition state TS-4 geometry in both directions, which verified that P3 and P4 linked the located transition state. In the TS-4, the N–H bond is stretched to 1.51 Å compared with the initial N–H bond length (1.02 Å). As the N–H bond elongates, the distance of C–N is shortened to 1.29 Å. The transition state TS-4 has a large energy-barrier height of 45.3 kcal/mol, but the reaction is exothermic by -10.1 kcal/mol. At the transition state TS-4, the hydrogen cyanide molecule is almost already formed. This is confirmed by the NPA results in which a triple bond character was found for C–N bond of HCN. In the next step, the adsorbed HCN can detach from the surface to yield the gaseous hydrogen cyanide molecule. However, the desorption energy of HCN from surface is found to be 37 kcal/mol, indicating the formation of gaseous hydrogen cyanide is kinetically unfavorable reaction. Thus, the reaction pathway R1 results in the cleavage of the N–Si bond and forms a HCN molecule and a hydrogenation product P4*, in which four hydrogen atoms are adsorbed above the SiCNT surface.

In addition to the N–H and C–H bonds cleavage, we investigated another possible reaction pathway R2 which involves the breaking of the C–N of methylamine on the surface. The optimized structure of stationary points is given in Figure 5. In the transition state (TS-5), the C···N bond distance is extended to 2.22 Å, and the distance of N–Si is shortened to 1.80 Å. At the same time, the $H_3C\cdots C_{surface}$ bond is reduced to 2.47 Å. A single imaginary frequency was computed, in which the corresponding vibrational mode has the characteristics of a reaction coordinate representing the C–N bond cleavage process. This step is exothermic by -4.8 kcal/mol and the energy barrier is as high as 73.5 kcal/mol, which indicates the impossibility of CH_3NH_2 decomposition in this pathway. Interestingly, compared with the methylamine decomposition process on the $B_{12}N_{12}$ cluster [28], the SiCNT slightly decreases the reaction energy barrier for the C–N bond scission by 8.0 kcal/mol. On the other hand, since the energy barrier for the side reaction that generates CH_3 and NH_2 fragments is relatively high; therefore, the generation of side products may be controlled by decreasing the temperature.

Finally, there are several concerns that need to be addressed regarding the feasibility of using SiCNTs in practical applications. The pristine and metal-free SiCNT possesses an efficient

catalytic activity toward the N–H and C–H bonds cleavage of CH_3NH_2. The reaction energies and the activation barriers obtained here suggest that for the decomposition of CH_3NH_2 on the SiCNT surface, the rate-determining step is HCNH → HCN + H. As a result, the reaction of CH_3NH_2 which produces a HCN molecule and four H atoms is likely to take place under normal conditions. Since for a SiCNT there are almost infinite Si–C bonds that each could act as a catalytic site, we believe that the cleavage and conversion of methylamine can take place to a large scale on SiCNTs, which may be useful for designing and developing metal-free catalyst based on SiCNTs.

4. Conclusion

In summary, the adsorption and decomposition of the CH_3NH_2 molecule on the surface of a pristine SiCNT has been studied using the DFT calculations. Equilibrium geometries and adsorption energies of the CH_3NH_2 adsorption on the surface of the SiCNT were identified. Our results revealed that CH_3NH_2 is adsorbed molecularly on the SiCNT surface through its nitrogen lone pair electrons in a top configuration with the adsorption energy of -45.6 kcal/mol. Two possible reaction pathways for CH_3NH_2 decomposition on the SiCNT surface were proposed. Our results indicated that the N–H and C–H scissions are the most favorable pathway on the SiCNT surface and the CH_3NH_2 dissociation on the nanotube surface is able to form a hydrogen cyanide molecule with a rate-controlling energy-barrier of 45.3 kcal/mol. Moreover, the routes R2 which generates the CH_3 and NH_2 fragments are highly endothermic. Hence, the side reaction can be depressed by decreasing the temperature.

References

1. L. Schlapbach, A. Zuttel, Nature 414 (2001) 353.
2. S. Satyapal, J. Petrovic, C. Read, G. Thomas, G. Ordaz, Catal. Today 120 (2007) 246.
3. E. Durgun, S. Ciraci, T. Yildirim, Phys. Rev. B 77 (2008) 085405.
4. R. Coontz, B. Hanson, Not so simple. Science 305 (2004) 957.
5. W. Liu, Y. H. Zhao, Y. Li, Q. Jiang, E. J. Lavernia, J. Phys. Chem. C 113 (2009) 2028.
6. P. Chen, Z.T. Xiong, J.Z. Luo, J.Y. Lin, K.L. Tan, Nature 420 (2002) 302.
7. W.Q. Deng, X. Xu, W.A. Goddard, Phys. Rev. Lett. 92 (2004) 166103.
8. J.Y. Lee, C.D. Wood, D. Bradshaw, M.J. Rosseinsky, A.I. Cooper, Chem. Commun. (2006) 2670.
9. P.M. Budd, A. Butler, J. Selbie, K. Mahmood, N.B. McKeown, B. Ghanem, K. Msayib, D. Book, A. Walton, Phys. Chem. Chem. Phys. 9 (2007) 1802.
10. J. Hannauer, U.B. Demirci, C. Geantet, J.-M. Herrmann, P. Miele, Int. J. Hydrogen Energy 37 (2012) 10758–10767.
11. G. C. Bond, Catalysis by Metals, New York: Academic Press, 1962.
12. K. A. Pearlstine , C. M. Friend, J. Am. Chem. Soc. 108 (1986) 5842.
13. L. Zhang, S. Li, Y. Tan, Z. Tang, Z. Guo, X. Yu, J. Mater. Chem. A 2 (2014) 10682.
14. D. E. Gardin, G.A. Somorjai, J. Phys. Chem. 96 (1992) 9424.
15. C. Q. Lv, J. Li, K.C. Ling, Z. F. Shang, G. C. Wang, Surf. Sci. 604 (2010) 779.
16. D. F. Johnson, Y. Wang, J. E. Parmeter, M. M. Hills, W. H. Weinberg, J. Am. Chem. Soc. 114 (1992) 4279.
17. M. E. Bridge, J. Somers, Vacuum 38 (1988) 317.

18. D. Jentz, M. Trenary, X. D. Peng, P. Stair, Surf. Sci. 341 (1995) 282.
19. C. Q. Lü, J. Li, S. X. Tao, K. C. Ling, G. C. Wang, J. Chem. Phys. 132 (2010) 044111.
20. J. Liu, C. Lü, D. Du, Y. Guo, J. Nat. Gas Chem. 21(2012) 132.
21. S. Y. Hwang, A. C. F. Kong, L. D. Schmidt, J. Phys. Chem. 93 (1989) 8327.
22. S. Y. Hwang , A. C. F. Kong , L. D. Schmidt, J. Phys. Chem. 93 (1989) 8327
23. D. F. Johnson , Y. Wang , J. E. Parmeter , M. M. Hills, W. H. Weinberg, J. Am. Chem. Soc. 114 (1992) 4279.
24. K.A. Pearlstine, C.M. Friend, J. Am. Chem. Soc. 108 (1986) 5842.
25. P.A. Thomas, R.I. Masel, J. Vac. Sci. Technol. A5 (1987) 1106.
26. J.J. Chen, N. Winograd, Surf. Sci. 326 (1995) 285.
27. R. Bafrali, A. T. Bell, Surf. Sci. 316 (1994) 267
28. M. D. Esrafili, R. Nurazar, Surf. Sci. 626 (2014) 44.
29. C. Pham-Huu, N. Keller, G. Ehret, M.J. Ledouxi J. Catal. 200 (2001) 400.
30. X. H. Sun, C. P. Li, W. K. Wong, N. B. Wong, C. S. Lee, S. T. Lee, B. K. Teo J. Am. Chem. Soc. 124 (2002) 14464.
31. R. Q Wu, M. Yang, Y. H. Lu, Y.P. Feng, Z. G. Huang, Q. Y. Wu, J. Phys. Chem. C 112 (2008) 15985.
32. M.D. Esrafili, H. Behzadi, J. Mol. Model. 19 (2013) 2375–2382.
33. M.W. Schmidt, K.K. Baldridge, J.A. Boatz, S.T. Elbert, M.S. Gordon, J.H. Jensen, S. Koseki, N. Matsunaga, K.A. Nguyen, S.J. Su, T.L. Windus, M. Dupuis, and J.A. Montgomery, J. Comput. Chem. 14 (1993) 1347.
34. M. Mirzaei, M. Mirzaei, J. Mol. Struct.: THEOCHEM 953 (2010) 134.
35. T. Yanaia, D.P. Tew, N. C. Handy, Chem. Phys. Lett. 393 (2004) 51.
36. A. J. Cohen, P. Mori-Sánchez, W. Yang, Chem. Rev. 112 (2012) 289.
37. R. Kobayashi, R.D. Amos, Chem. Phys. Lett. 420 (2006) 106–109.
38. A. E. Reed, L. A. Curtiss, F. Weinhold, Chem. Rev. 88 (1988) 899.
39. J.X. Zhao, Y. H. Ding, J. Chem. Theory Comput. 5 (2009) 1099.
40. X. Wang, K. M. Liew, J. Phys. Chem. C 115 (2011) 10388.

Table 1. The adsorption energies (E_{ad}), change of Gibbs free energies (ΔG_{298}), change of enthalpies (ΔH_{298}), net charge transfer (q_{CT}) and band gap (E_g) of CH_3NH_2–SiCNT configurations

configuration	E_{ad} (kcal/mol)	ΔG_{298} (kcal/mol)	ΔH_{298} (kcal/mol)	q_{CT} (e)	E_g (eV)
A	-45.6	-26.4	-38.5	0.29	2.14
B	-1.6	5.5	-2.5	0.07	1.97

Table 2. Calculated activation energies (E_{act}), imaginary frequencies (ν), reaction energies (ΔE), change of Gibbs free energies (ΔG_{298}), change of enthalpies (ΔH_{298}) of decomposition of CH_3NH_2 on the SiCNT surface

reaction	E_{act} (kcal/mol)	ν (cm^{-1})	ΔE (kcal/mol)	ΔG_{298} (kcal/mol)	ΔH_{298} (kcal/mol)
Pathway R1					
A→ P1	7.0	1567i	-23.8	-24.1	-23.7
P1→P2	13.4	645i	-3.2	-3.0	-3.3
P2→P3	25.8	1187i	20.8	20.9	20.8
P3→P4	45.3	1526i	-9.6	-8.7	-10.2
P4→P4*	-	-	36.8	24.8	38.4
Pathway R2					
A→ P5	73.5	728i	-4.8	-7.4	-7.0

Figure 1. Optimized structure and electronic density of states (states/eV) of pristine SiCNT and CH_3NH_2–SiCNT complexes. All distances in Å. Color code for each optimized structure: gray ball: C; blue-green ball: Si; blue ball: N; white ball: H. In the DOS plots, the dashed vertical lines mark the Fermi levels.

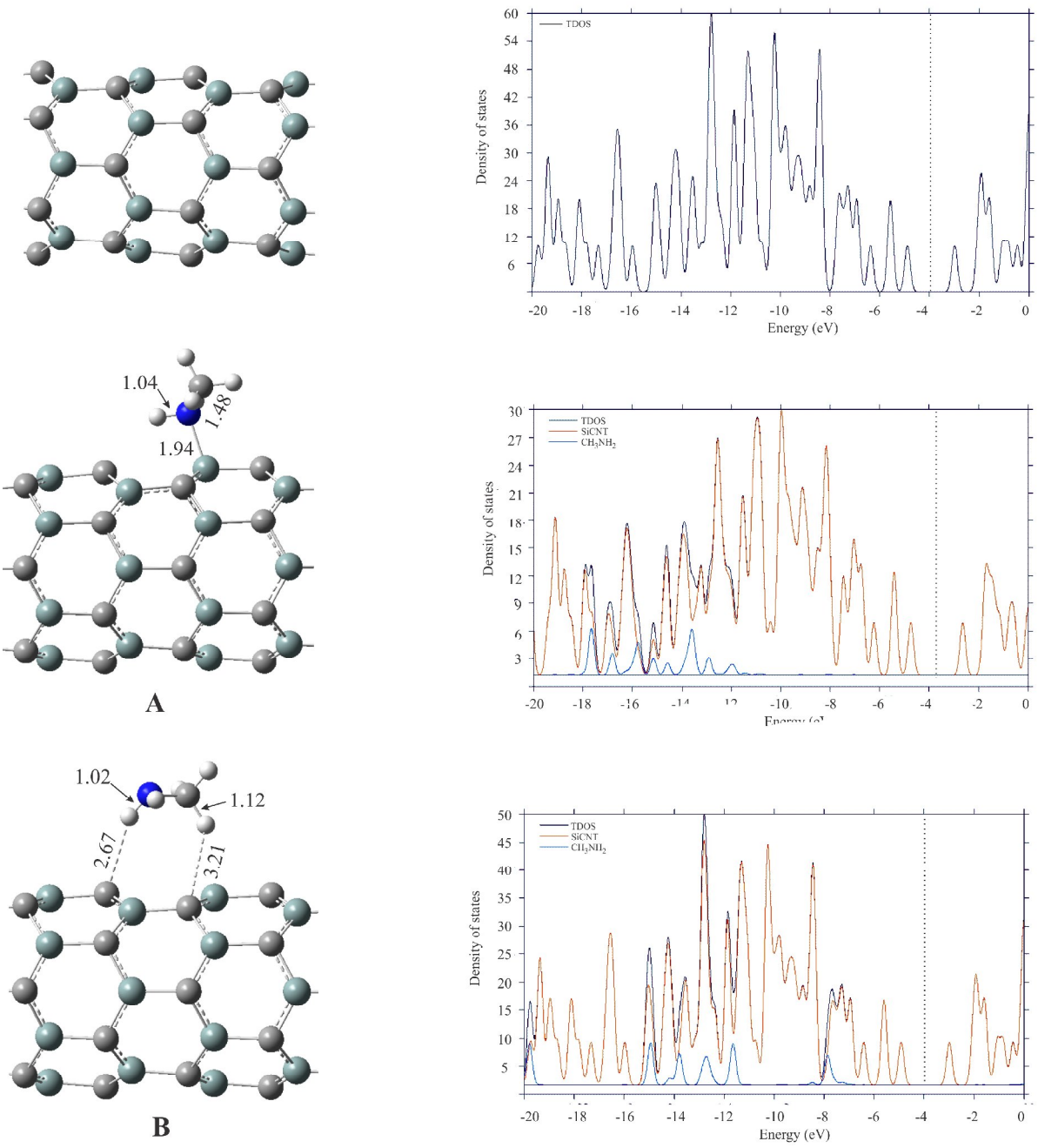

Figure 2. Figure 2. Electronic density difference isosurfaces (0.001 e/Å^3) for CH_3NH_2–SiCNT complexes. The blue region shows electron accumulation, while the red region shows electron loss.

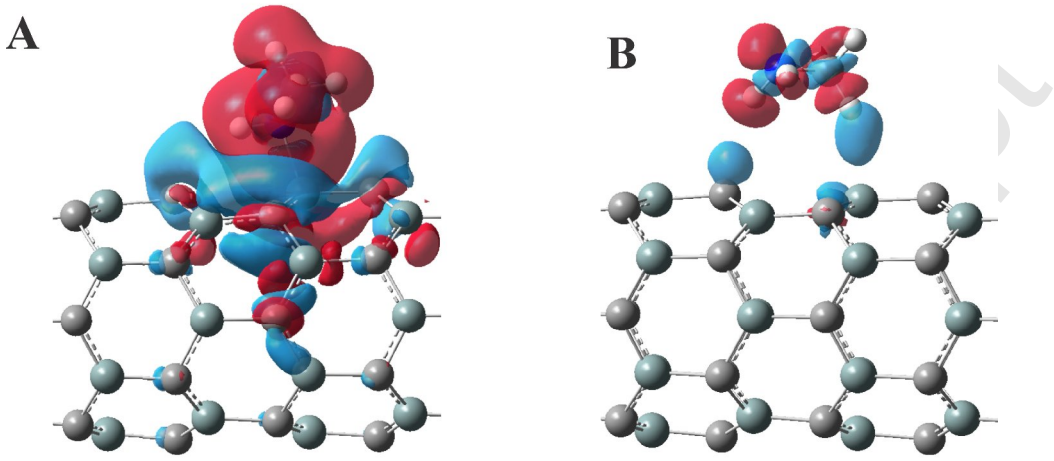

Figure 3. Reaction pathways (R1 and R2) of CH_3NH_2 decomposition on the SiCNT surface

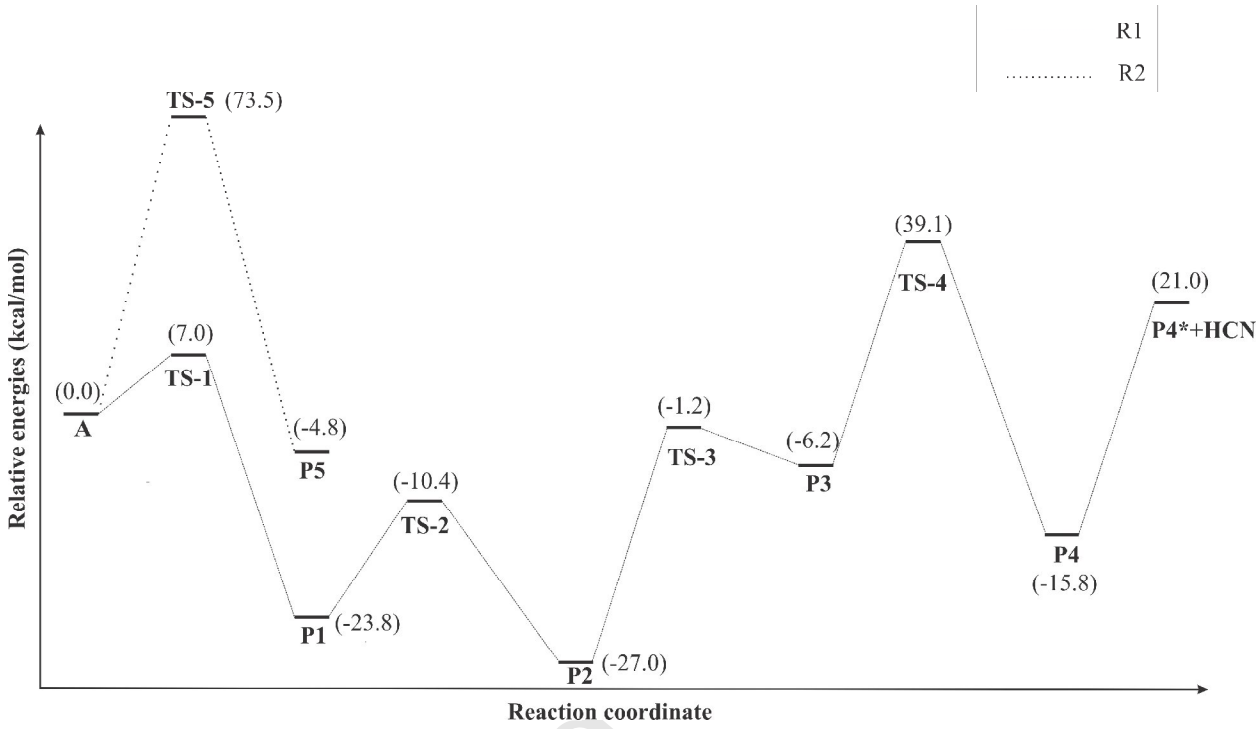

Figure 4. Optimized structure of stationary points for reaction channel R1. All distances are in Å.

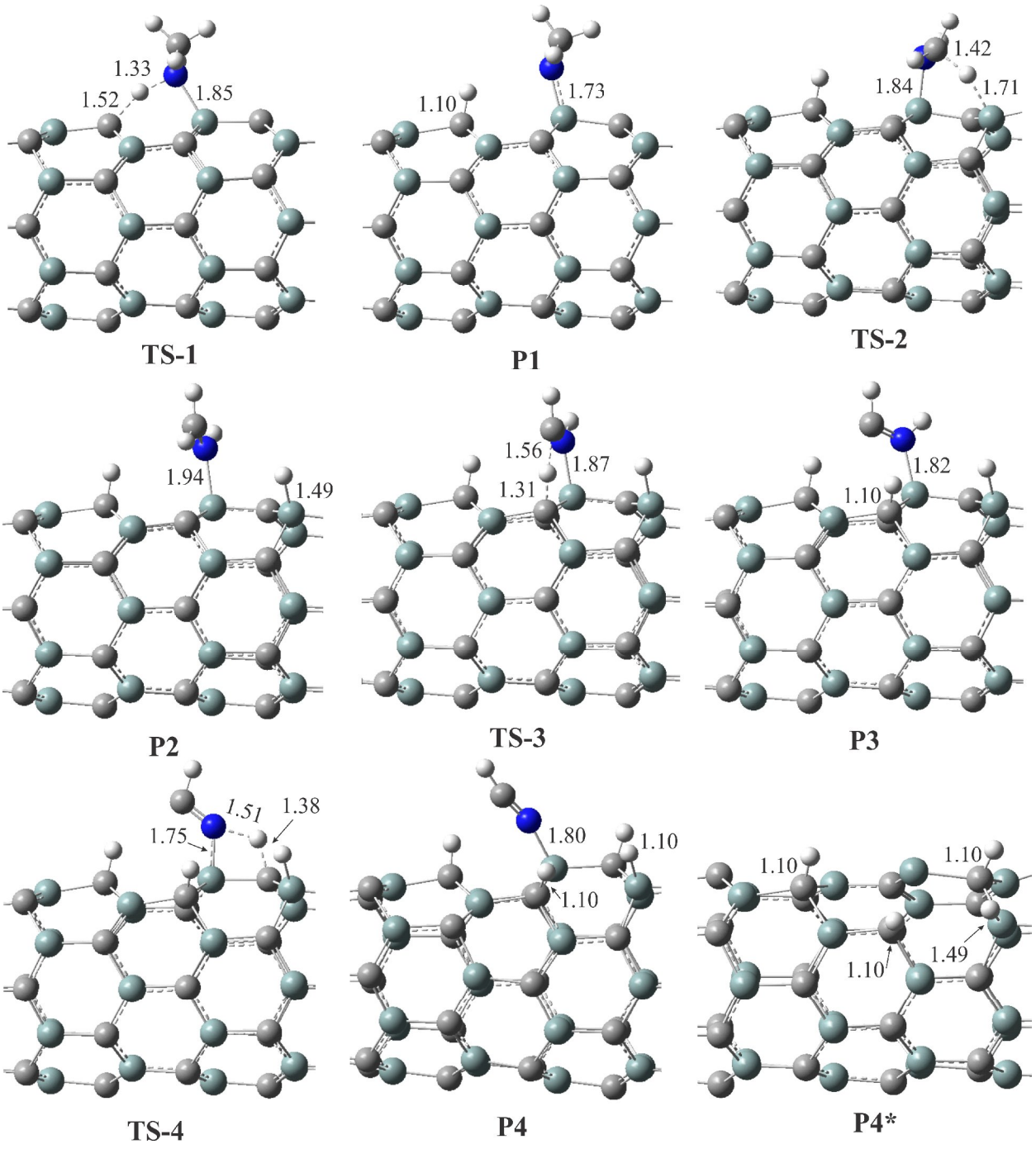

Figure 5. Optimized structure of stationary points for reaction channel R2. All distances are in Å.